EXTRACTING URBAN DEPRIVATION INDICATORS USING SUPERSPECTRAL VERY-HIGH-RESOLUTION SATELLITE IMAGERY

Stefanos Georganos[1], Sabine Vanhuysse[1], Ángela Abascal [2], Monika Kuffer[3]

[1] Department of Geosciences, Environnement and Society, Université Libre De Bruxelles (ULB), Brussels, Belgium
[2] Faculty of Architecture, Universidad de Navarra, Pamplona, Spain
[3] Department of Urban and Regional Planning and Geo-Information Management, Faculty of Geo-Information Science and Earth Observation, University of Twente, Twente, Netherlands

IGARSS 2021 - 2021 IEEE International Geoscience and Remote Sensing Symposium | 978-1-6654-0369-6/21/$31.00 ©2021 IEEE | DOI: 10.1109/IGARSS47720.2021.9554849

ABSTRACT

Most research pertaining to mapping deprived urban areas is limited to locating and delineating deprived area's extents within and across cities. In this work, we go beyond and characterize deprived areas by utilizing a wide suit of remotely sensed predictors to map the intra-urban distribution of land cover (LC) in deprived communities in Nairobi, Kenya. We assess the contribution of WorldView-3 (WV-3) multispectral and shortwave infrared bands for the task of deprived urban areas land cover classification at a very-high-resolution scale. Our results highlight the potential of WV-3 to accurately map the LC while the potential of intra-urban transferability was shown to be satisfactory. Moreover, feature selection dramatically decreased the computational complexity of the LC models with no losses in classification accuracy. We propose a set of indicators such as the density of garbage piles to be extracted at an aggregated grid level. This aggregation helps characterize urban deprivation at a fine scale and assist local authorities and stakeholders in implementing evidence-based policy making.

Index Terms— urban deprivation, slums, land cover, remote sensing, machine learning, urban health

1. INTRODUCTION

Sub-Saharan African (SSA) cities have been undergoing rapid and uncontrolled urbanization in the past decades. By 2050, about 60% of its population is projected to reside in cities [1] while the overall population will have doubled. The undergoing changes in urban environments have intensified socio-economic spatial segregation within SSA cities [2]. This can be clearly expressed by the proliferation and expansion of deprived urban areas or so-called "slum" neighborhoods [3]. For instance, and as defined by the United Nations (UN) Habitat, a "slum household" lacks one or more of the following: adequate sanitation, security of tenure, durable housing, access to safe water and adequate living space [4]. Additionally, slum neighborhoods are often disproportionally affected by disease burden and increased mortality compared to population residing in the more affluent parts of the city [5]. For example, malaria, a common disease in the SSA region, was positively linked with the presence of deprived settlements in the cities of Kampala (Uganda) and Dar es Salaam (Tanzania) [6]. Moreover, slum communities have been greatly neglected during the COVID-19 pandemic, being "masked out" of measurements access to healthcare. Communities are facing immense challenges with waste management, while the global disruption of product transportation networks has affected them dramatically [7], [8]. The UN Sustainable Development Goals (SDG) 11 is one of the most large-scale efforts to improve the well-being of urban residents and their quality of life. To help achieve its objectives, multi-faceted levels of information are needed, particularly for the most vulnerable and deprived urban areas. As SSA suffers from data scarcity, parts of the required information relating to physical, socio-economic, demographic and health factors can be derived from Earth Observation (EO) [9], [10].

Most EO-based studies regarding deprived urban areas are focused on locating and delineating them [3], [11]–[13] with few efforts to highlight and understand intra-slum characteristics and deprivation levels. An important aspect contributing to the understanding of deprivation levels and urban health relates to waste management as the accumulation of waste is very problematic inside slums areas. In this study, we select a set of deprived settlements in the city of Nairobi, Kenya and attempt to map and extract potentially useful indicators to characterize their urban structure with a wide suit of satellite information. We aim to assess the contribution of the full WorldView-3 MS and SWIR arsenal for the task of intra-slum land cover (LC) mapping through a Geographic Object-Based Image Analysis (GEOBIA) framework and a parsimonious computational framework.

2. MATERIALS AND METHODS

2.1 Study area and satellite information

We utilized a dataset, produced by Spatial Collective (SC), which contains locations and extents of deprived urban areas across the city, collected by local experts. For training the EO models, the region of interest is an area encapsulating the communities living in Mathare (Nairobi, Kenya) one of the cities informal settlements. Mathare consists of 13

expert-delineated neighborhoods (1,43 km^2). With respect to the satellite information, we made use of orthorectified WorldView-3 (WV-33) panchromatic (0.30m), multispectral (MS; 8 bands, 1.20m), and shortwave infrared (SWIR) (8 bands, 3.70m) data covering the study area, collected in 2019. The WV-3 multispectral bands were pansharpened through the PANSHARP module of the PCI Geomatica software. Additionally, we co-registered the WV-3 SWIR bands to the WV-3 multispectral bands as a mild shift existed between them. The study area and is depicted in Fig. 1, showing a false-color multispectral composite.

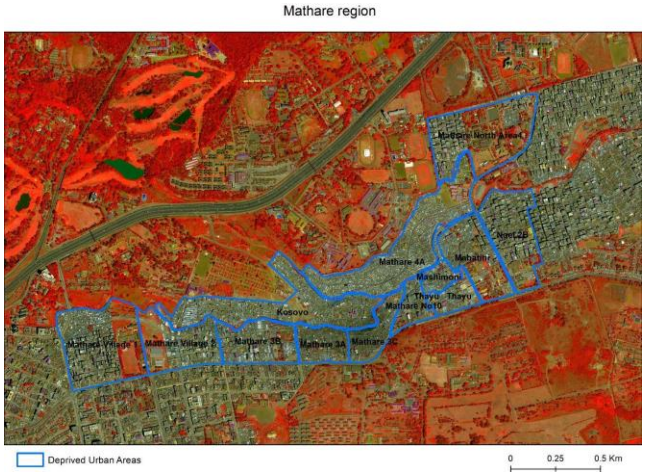

Figure 1. Mathare slum where the collection of data and training of the LC models took place, visualized through a false-color composite of WorldView-3 bands.

2.2 Training data

Using computer assisted photo interpretation, we labelled 6240 points within the study area with the corresponding LC category and their associated area-level domain of deprivation (Table 1). The reason for this extensive collection of training data was i) to have a large amount of information to develop a robust semi-automated processing chain and ii) investigate transferability of the models in the rest of the slum regions in Nairobi. With respect to the LC legend, among standard class nomenclature, we identified classes of potential use for our objectives such as vehicles and garbage piles. Mapping garbage piles is a strong request from communities and researchers due to the health impact of solid waste, during the COVID-19 crisis.

2.3 Geographic-Object-Based Image Analysis (GEOBIA)

As a first step, we applied our semi-automated segmentation processing chain on Mathare. Utilizing unsupervised segmentation parameter optimization we fine-tuned the parameters of a region-growing segmentation algorithm [14] implemented in the open-source GRASS GIS software as proposed by Grippa et al. [15] using as input the multispectral bands of the WV-3 imagery. Afterwards, we extracted a set of image predictors at the segment level to be used as input to the classification algorithms. To make sure that most of the relevant information for the LC exercise would be extracted, we computed several thousand of potentially useful predictors. With respect to the WV-3 multispectral data, for each segment, we extracted descriptive statistics (i.e., mean, median, 1st and 3rd quartiles, variance, standard deviation, minimum, maximum) for each band and the Normalized Difference Vegetation Index (NDVI). Additionally, we extracted the same type of statistics for a wide set of textures calculated in various window sizes (3,9,19). Finally, to further enhance the inclusion of contextual information, for each segment, we computed neighboring information (mean and standard deviation) of adjacent spectral elements. This led to a total of 10813 predictive features coming from the WV-3 MS data available as initial input to the classification task. A similar approach was adopted for the SWIR bands, except that only a small window was retained for the texture (3) leading to a total of 3360 predictors. The window size was adapted taking into account the coarser spatial resolution of the SWIR bands.

Table 1. Land cover classes and training data

Class	Deprivation domain (aspect) captured - proxy	Samples
Building	Unplanned morphology	2839
Tall vegetation	Environmental asset	249
Low vegetation	Environmental asset	186
Vehicle (i.e., car)	Road infrastructure	270
Ground surface	Unplanned morphology	842
Garbage piles	Health-related hazards	149
Water	Physical and health-related hazard	28
Shadow	Unplanned morphology	414

2.4 Feature selection and classification

As pointed out in recent work [16], feature selection (FS) is a necessary preparatory step in the face of an exceedingly large predictor dataset, as it helps drastically reduce further computational burden and data management, potentially improve classification accuracy and finally, create more parsimonious and more transferable models. To do so, we deployed the Variable Selection Using Random Forest (VSURF) algorithm as proposed by Genuer et al. [17]. VSURF is tailored to handle datasets with large number of predictors and identify a subset of the most discriminant ones. VSURF utilizes the RF-derived mean decrease in classification accuracy as a measure to select relevant and discriminant features through iterative model training. To compare the potential contribution of the various WV-3 bands we investigated the contribution of the first 3 MS bands (RGB), 4 MS bands (RGBNIR), the full multispectral bundle (denoted as MS-8) and finally, using the full dataset, including SWIR information (denoted as All). By applying VSURF to each of our datasets we reduced the complexity

of the models by orders of magnitude (RGB 21 features; RGBNIR 27 features; MS-8 26 features; ALL 28 features). Texture prevalence was over 50% in the RGB and RGBNIR models while MS-8 and ALL datasets included lower texture fraction due to the addition of unique spectral information. NDVI related features were distributed similarly across datasets (RGBNIR and MS-8 23%; ALL 18%). Finally, we used a RF classifier to train the models before and after FS.

3. RESULTS

3.1 Land cover classification

To validate the results on the training area (Mathare), we used the Out of Bag (OOB) accuracy extracted from the RF classifier, a robust performance indicator, similar to an independent test set. The results of our experiments are shown in Table 2. Notably, FS models are dramatically more computationally efficient during the training stage of the classifier, without any visible reduction in accuracy. As such, only FS-based models were retained for further analysis. Using the visible and near-infrared bands (RGBNIR) is the best choice when it comes to jointly account for accuracy but also computational efficiency while the SWIR bands did not appear to bring significant gains to the classification accuracy, potentially due to the large mismatch between the spatial resolution of the SWIR-MS datasets (3,7 meters, 0,33 meters).

Table 2. Overall accuracy and training time for the various classification experiments. *FS* indicates a model where VSURF feature selection has been applied.

Source	Overall accuracy (%)	Training time (s)
All FS	89.4	7.62
All	89.9	99.00
MS-8 FS	89.2	5.20
MS-8	89.5	80.04
RGBNIR FS	89.2	6.57
RGBNIR	89.5	58.60
RGB FS	85.2	49.88
RGB	86.1	376.00

3.2 Transferability experiments

To assess the transferability potential of our models, we apply them to predict LC within other deprived areas in the city of Nairobi and validate them using an independent test set totaling 3000 points. There does not appear to be significant improvements when including all 8 WV-3 MS bands compared to using only 4. Overall, the MS models produced very high accuracy for built-up segmentation, which is the most dominant class in the LC scheme (Table 3). The classification of buildings and vegetation is remarkably good, highlighting the efficiency of the WV-3 bands for mapping the urban fabric (Table 2; Fig. 2). The classification of garbage piles and water is more complex, yet satisfactory, even though issues of misclassifications appear. SWIR-based models produced higher accuracies for classes such as buildings and garbage piles. This can be linked to the ability of SWIR sensors to capture a large variety of physical materials (iron, rusty iron, types of plastic) in these classes.

3.3 Extraction of indicators relevant to urban deprivation

As indicated by survey results within the scope of the SLUMAP (http://slumap.ulb.be/) project, the most user desired indicators regarding intra-slum and deprivation indicators were related to building/density and openness. We extracted gridded products for several LC classes, while we also investigated the additional information that landscape metrics might bring on the table. As a proof of concept, in Fig. 3, we present a gridded product of garbage pile density across Mathare, which among other indicators (such as building and vegetation density) can be used to measure and characterize urban deprivation. The process for extracting gridded products is based on an automated processing chain using Python and GRASS GIS in Jupyter Notebook. These indicators might help characterize the socio-physical typology of deprived areas and due to their gridded format, can easily be aggregated according to other available boundaries (i.e., census units, expert delineations).

Table 3. Overall and class accuracy for the various classification experiments on an independent test set in other deprived areas of the city.

Class	ALL	MS-8	RGBNIR	RGB
Overall Accuracy	83.5	**82.9**	**82.9**	75.6
Building	**89.0**	87.1	87.6	82.3
Bare soil	**74.9**	73.6	71.0	60.6
Low vegetation	86.5	**86.9**	85.9	70.2
Trees	82.2	**83.8**	82.4	74.2
Shadow	80.8	83.0	**84.0**	82.1
Vehicle	93.1	94.8	**97.0**	92.8
Water	55.9	57.1	**64.1**	60.9
Garbage piles	**79.2**	**79.2**	76.5	61.8

4. CONCLUSION

We propose a GEOBIA-based framework to map urban deprivation indicators through a tailored LC classification scheme employing various WV-3 data. Our results suggest

that the RGBNIR bands are suitable to map deprived areas LC but adding SWIR information may help with the classification of complex and important classes such as buildings and garbage waste. Future work is expected to tackle transferability of this framework across cities and dig further in characterizing and extracting urban deprivation indicators.

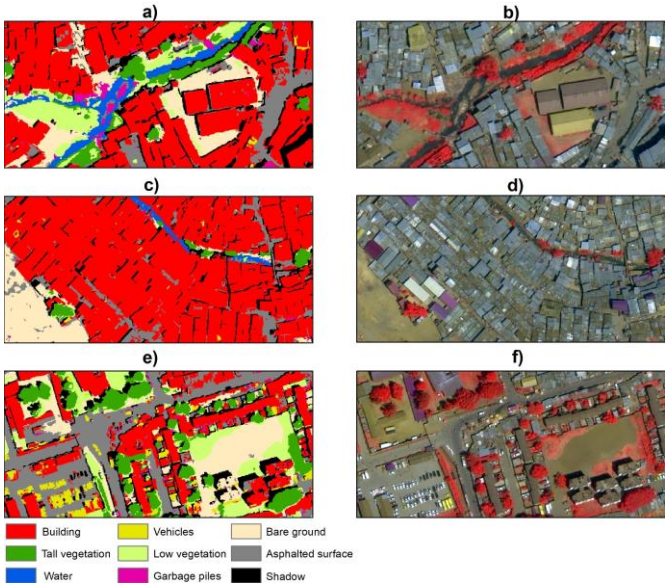

Figure 2. Subsets of the LC map (multispectral WV-3. 4 bands) in various environments. a) Garbage piles across the river. c) densely built neighborhoods. e) vehicles in a planned neighborhood

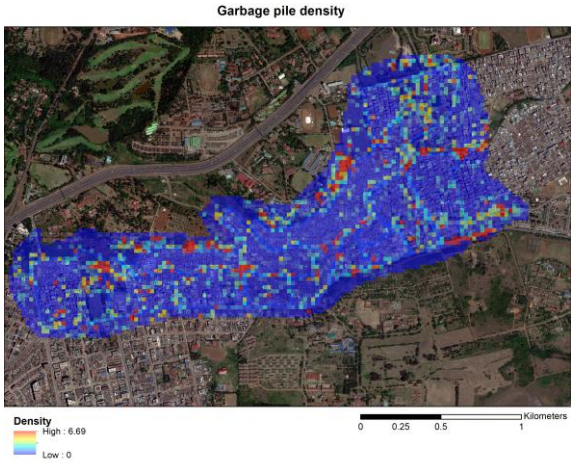

Figure 3**.** Example of gridded indicators from the LC maps. Garbage waste density in Mathare. Nairobi.

5. AKNOWLEDGEMENTS

The research pertaining to these results received financial aid from the Belgian Federal Science Policy (BELSPO) according to the agreement of subsidies no. SR/11/380 and SR/00/337.

6. REFERENCES

[1] U. Nations, "World Urbanization Prospects: The 2014 Revision, Highlights. Department of Economic and Social Affairs," Popul. Div. United Nations, 2014.
[2] E. Wolff et al., "Diversity of urban growth patterns in Sub-Saharan Africa in the 1960--2010 period," African Geogr. Rev., vol. 39, no. 1, pp. 45–57, 2020.
[3] M. Kuffer, K. Pfeffer, and R. Sliuzas, "Slums from Space — 15 Years of Slum Mapping Using Remote Sensing," 2016.
[4] United Nations Human Settlements Programme (UN-Habitat), "Distinguishing slum from non-slum areas to identify occupants' issues," News, 2017. .
[5] R. Lilford et al., "Because space matters: conceptual framework to help distinguish slum from non-slum urban areas," BMJ Glob. Heal., vol. 4, no. 2, p. e001267, 2019.
[6] S. Georganos et al., "Modelling and mapping the intra-urban spatial distribution of Plasmodium falciparum parasite rate using very-high-resolution satellite derived indicators," Int. J. Health Geogr., vol. 19, no. 1, pp. 1–18, 2020.
[7] S. Mollah and Z. Islam, "Dhaka Slums: Where Covid is curiously quiet," 2020.
[8] P. L. Brito et al., "The Spatial Dimension of COVID-19: The Potential of Earth Observation Data in Support of Slum Communities with Evidence from Brazil," ISPRS Int. J. Geo-Information, vol. 9, no. 9, p. 557, 2020.
[9] D. R. Thomson et al., "Need for an Integrated Deprived Area 'Slum' Mapping System (IDEAMAPS) in Low-and Middle-Income Countries (LMICs)," Soc. Sci., vol. 9, no. 5, p. 80, 2020.
[10] M. Kuffer et al., "The Role of Earth Observation in an Integrated Deprived Area Mapping System for Low-to-Middle Income Countries," Remote Sens., vol. 12, no. 6, p. 982, 2020.
[11] M. Kuffer, R. Sliuzas, K. Pfeffer, and I. Baud, "The utility of the co-occurrence matrix to extract slum areas from {VHR} imagery," in 2015 {Joint} {Urban} {Remote} {Sensing} {Event} ({JURSE}), 2015, pp. 1–4.
[12] D. Kohli, R. Sliuzas, N. Kerle, and A. Stein, "An ontology of slums for image-based classification," Comput. Environ. Urban Syst., vol. 36, no. 2, pp. 154–163, 2012.
[13] R. Engstrom, D. Pavelesku, T. Tanaka, and A. Wambile, "Mapping Poverty and Slums Using Multiple Methodologies in Accra, Ghana," in 2019 Joint Urban Remote Sensing Event (JURSE), 2019, pp. 1–4.
[14] M. Lennert and G. D. Team, "Addon i.segment.uspo," Geogr. Resour. Anal. Support Syst. SoftwareVersion 7.3, 2016.
[15] T. Grippa, M. Lennert, B. Beaumont, S. Vanhuysse, N. Stephenne, and E. Wolff, "An Open-Source Semi-Automated Processing Chain for Urban Object-Based Classification," Remote Sens., vol. 9, no. 4, p. 358, 2017.
[16] S. Georganos et al., "Less is more: optimizing classification performance through feature selection in a very-high-resolution remote sensing object-based urban application," GIScience Remote Sens., pp. 1–22, Nov. 2017.
[17] R. Genuer, J.-M. Poggi, and C. Tuleau-Malot, "VSURF: An R Package for Variable Selection Using Random Forests," R J., vol. 7, no. 2, pp. 19–33, 2015.